17th Brazilian Congress of Thermal Sciences and Engineering
November 25th-28th, 2018, Águas de Lindóia, SP, Brazil

ENCIT-2018-0255
SIMULATION OF THREE-DIMENSIONAL FLOW OF AIR IN DUCT OF INDUSTRIAL TERM-SHRINKING TUNNEL

Diego Pavan
Rubieli Carla Frezza Zeferino
Universidade Comunitária da Região de Chapecó – Unochapecó, Mechanical Engineering Department
Servidão Anjo da Guarda, 295 D, Efapi, CEP 89809-900, Chapecó – SC, Brazil
pavan.diego@unochapeco.edu.br
rubifrezza@unochapeco.edu.br

André Luiz Grando Santos
Marcos Roberto Fedrizzi
Universidade Comunitária da Região de Chapecó – Unochapecó, Mechanical Engineering Department
Servidão Anjo da Guarda, 295 D, Efapi, CEP 89809-900, Chapecó – SC, Brazil
andreluizgrando@unochapeco.edu.br
marcos.fedrizzi@unochapeco.edu.br

Abstract. *This works purpose is to study the air flow inside of a lateral duct of an industrial term-shrinking tunnel using computational fluid dynamics (CFD). The results showed a formation of recirculation zones, contraction and expansion occurs along the flow, as a function of fluid trajectory change. The definition of points to fluid trajectory analysis influences the result due to the distance between the points. The velocity gradient is a function of the chosen mesh. The mesh refinement increase tends to approximate the model to experimental data, however, very refined meshes tend to cause higher oscillations in the model. These results allow to conclude that the model obtained in CFD can be used to represent the real flow, supporting future studies to optimize the equipment operating conditions.*

Keywords: *internal flow, computational fluid mechanics, finite element method, air velocity, SWFS*

1. INTRODUCTION

The development of research that uses computational fluid dynamics (CFD) to evaluate real equipment is increasing in the literature. The CFD base owns advanced algorithms and has been used in works developed by Frikha *et al*. (2015), Stefan and Gunther (2016), Castorani *et al*. (2016), Turner *et al*. (2017), Bianchi *et al*. (2017), Lorusso *et al*. (2017), Prah and Yun (2017), Mei *et al*. (2018) to analyze problems of different complexities.

Jeong and Seong (2014) describe that CFD base is able to implement the finite volume method (FVM), finite element method (EFM) and finite difference method (FDM). In work developed by Kempe and Hantsch (2017) and by Delgado *et al*. (2017), the FVM was used to solve systems of partial differential equations in flowing of geometries with high complexity.

SolidWorks Flow Simulation (SWFS) is an integrated CFD computing base that uses the finite volume method, cartesian base with orthogonal planes to their respective axes, immersed body mesh and conservation laws of mass, momentum and energy (Sobachkin and Dumnov, 2013). The fluid mechanics problems solving using SWFS has been studied by Ragoth Singh *et al*. (2013), Ragoth Singh and Nataraj (2014), Driss *et al*. (2014), Wang *et al*. (2017), Busto *et al*. (2018) and heat transfer by Shrikant *et al*. (2016).

In this context, the present work aims to evaluate the air flow in a directional duct of an industrial term-shrinking tunnel using computational fluid dynamics. The air flow behavior in the lateral duct is important because it is through it that the air reaches the chamber where term-shrinking process occurs.

2. METHODOLOGY

The present work involves the simulation analysis of the internal air flow in a lateral duct of an industrial equipment term-shrinking.

2.1 Mathematical modeling

Flow of a fluid can be analyzed through the equations of mass conservation and momentum laws presented in the literature. When a fluid particle is analyzed in three-dimensional flow, the conditions are highly complex, being generally analyzed through the solution of the Navier-Stokes equations (Fox and McDonald, 2014).

From the average velocity, Reynolds number described in Eq. (1) is determined, which can be laminar or turbulent.

$$\mathrm{Re}_{D_h} = \frac{\rho \cdot u_m \cdot D_h}{\mu} \tag{1}$$

D_h is the hydraulic diameter of the duct (m), u_m is the mean flow velocity of the fluid (m.s^{-1}), ρ is the specific mass of the fluid (kg.m^{-3}) and μ is the dynamic viscosity of the fluid (Pa.s).

The hydraulic diameter can be expressed by Eq. (2).

$$D_h \equiv \frac{4 \cdot A_{tr}}{P} \tag{2}$$

A_{tr} is the cross-sectional area of the flow (m^2), P is the wet perimeter (m).

Assuming the fluid is incompressible, and a stationary state, the law of conservation of mass can be written according to Eq. (3).

$$\nabla \cdot \overline{V} = 0 \tag{3}$$

∇ is the Laplacian operator and $\overline{V}$ is the velocity vector in directions ($\bar{i}u + \bar{j}v + \bar{k}w$) (m.s^{-1}).

2.2 Reference geometry

The model of industrial term-shrinking tunnel 3D, in different views, obtained by SolidWorks 2015, is shown in Fig. 1 and Fig. 2, (a) and (b).

The lateral duct for computational scale study is presented in Fig. 3. Its dimensions are: H1 = 416.5 mm, H2 = C2 = 50.0 mm, C1 = 70.0 mm, L1 = 600.0 mm and S4 = 170 holes with a diameter of 5.0 mm and the wall thickness of the solids is 1.50 mm. The airflow input in duct occurs by H1 and output by S4.

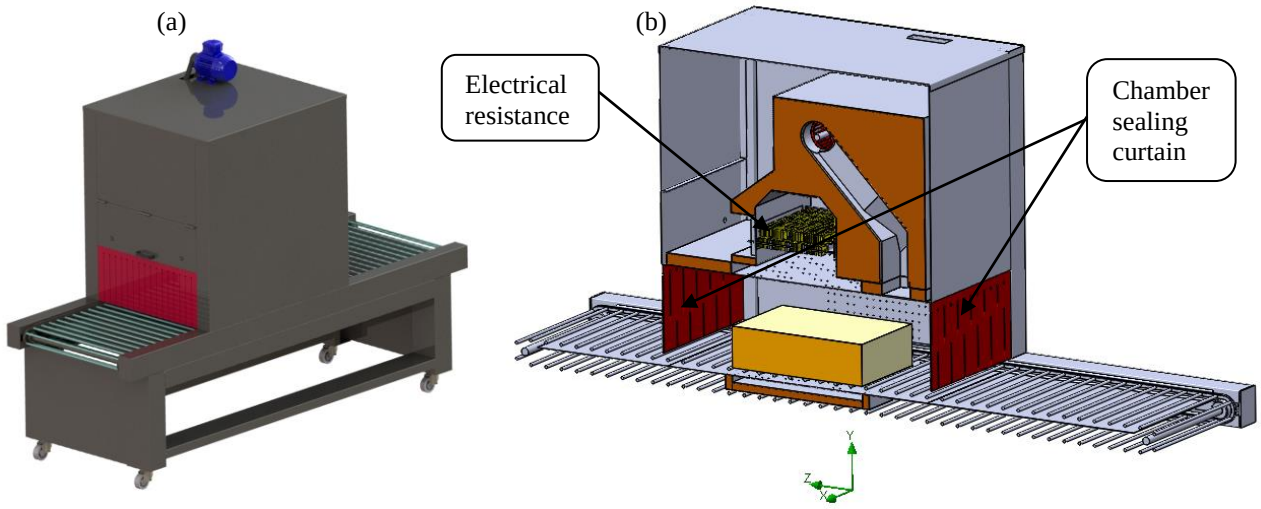

Figure 1. (a) Generic isometric tunnel model and (b) Total isometric tunnel model cut

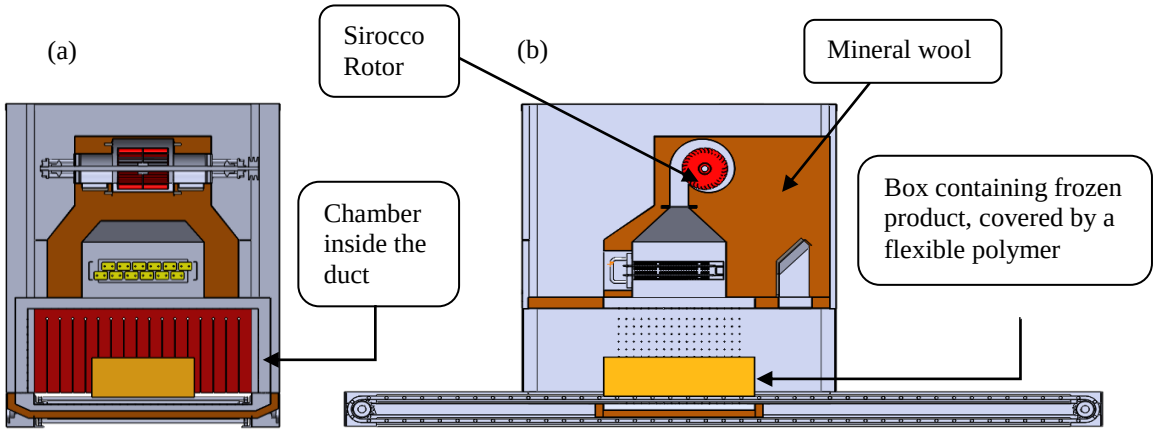

Figure 2. (a) Full cut in width and (b) Total cut in length

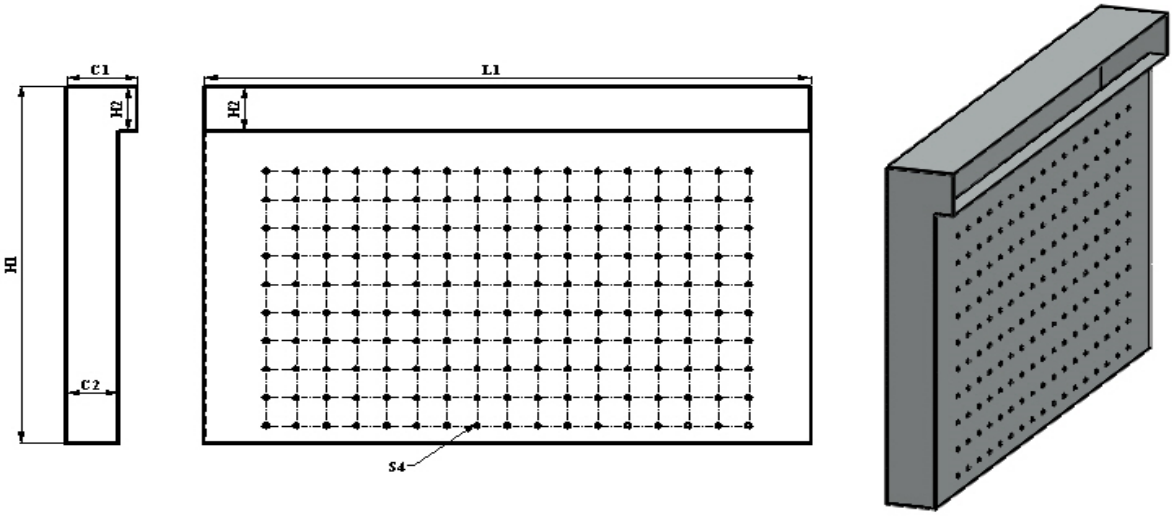

Figure 3. Detailing lateral duct of the term-shrinking tunnel

2.3 Computational model and boundary conditions

Scale model data entered in the software is shown in Table 1.

Table 1. Definition of the computational model

Description	Configuration
Project name	Duct side of the term shrink tunnel
System of units	SI
Type of analysis	Internal; Exclude cavities with no flow condition
Physical characteristics	Gravity (component y = -9,81 m.s^{-2})
Reference axis	X
Fluid Type	(Air) fluid and its properties available in the Solidworks library
Flow condition in the system	Laminar Only
Initial condition of solid material	The simple carbon steel material was used in the Solidworks library
Standard thermal condition of the wall	Adiabatic wall
Roughness of material	60 µm
Thermodynamic parameter 01	Pressure = 101325 Pa
Thermodynamic parameter 02	Standard temperature 14,5 °C
Initial velocity parameter	Velocity in the directions (x = 0 m.s^{-1}; y = 0 m.s^{-1}; z = 0 m.s^{-1})

The boundary conditions used at the simulation are presented in Table 2 and can be visualized in Fig. 4.

Table 2. Boundary Conditions

Description	Configuration
Computational domain	Three-dimensional simulation
Inlet Velocity	u_m= 0.166 m.s^{-1}; Profile uniform face to face; P = 101325 Pa; T = 14.5 °C; Reference axis = X (normal to entry face).
Environment Pressure	Pressure of the environment = 101325 Pa; T = 14.5 °C; Reference axis = X (normal to output face).

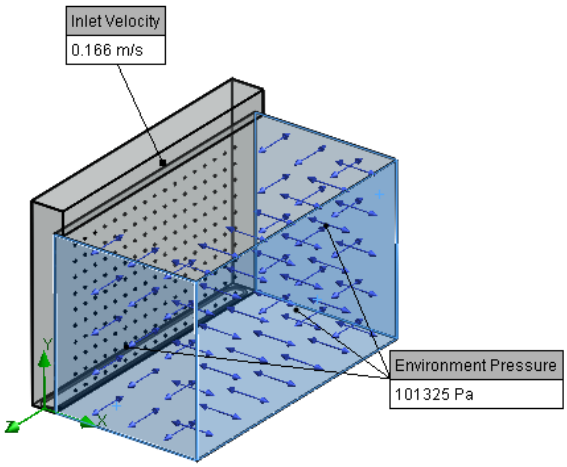

Figure 4. Location of boundary conditions

The flow in lateral duct was analyzed changing the mesh as described at Table 3. To the mesh refinement, it was used a minimum channel opening of 5.0 mm and minimum wall thickness of 1.50 mm.

Table 3. Base mesh

Axis direction	Computational domain (m)	Mesh 01[(1)] (Number of cells)	Mesh 02[(2)] (Number of cells)	Mesh 03[(3)] (Number of cells)	Mesh 04[(4)] (Number of cells)
X	0.34380	10	18	38	52
Y	0.41546	10	22	42	58
Z	0.60120	14	30	62	86

[(1)] Automatic level 1, [(2)] Automatic level 3, [(3)] Automatic level 5 e [(4)] Automatic level 8.

The definition of the computational mesh is characterized at Figs. 5, 6, 7 and 8, which show the cells distribution at the geometry in the XY plane and the refinement at specific points mainly in the aperture S4, which is the output of air from duct.

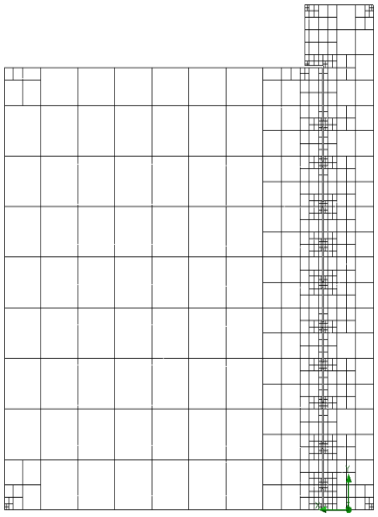

Figure 5. Cells distribution to mesh 01

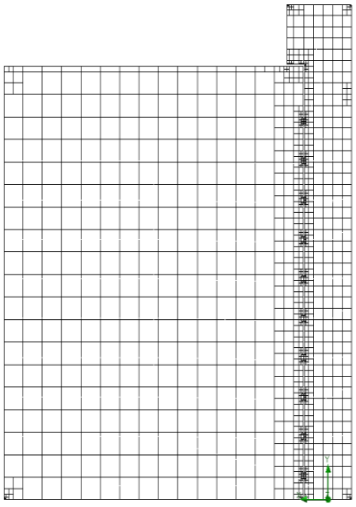

Figure 6. Cells distribution to mesh 02

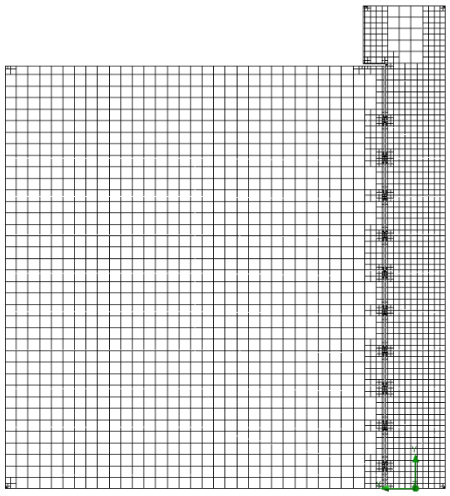

Figure 7. Cells distribution to mesh 03

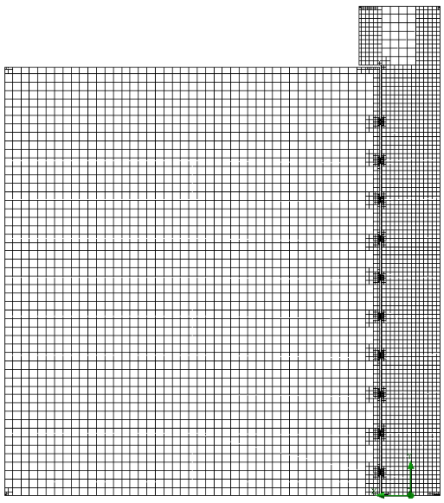

Figure 8. Cells distribution to mesh 04

The number of cells present in the computational domain for each mesh is described in Table 4.

Table 4. Mesh size

Description	**Mesh 01 (Number of cells)**	**Mesh 02 (Number of cells)**	**Mesh 03 (Number of cells)**	**Mesh 04 (Number of cells)**
Fluid cells	29271	75028	231708	662448
Partial cells	29639	70947	139960	202623
Total cells	58910	145975	371668	865071

3. RESULTS

3.1 Simulation results

The simulation results to velocity gradients and to representation of air trajectories, as a function of the meshes 01, 02, 03 and 04 are shown at Fig. 9, 10, 11, 12, 13, 14, 15 and 16.

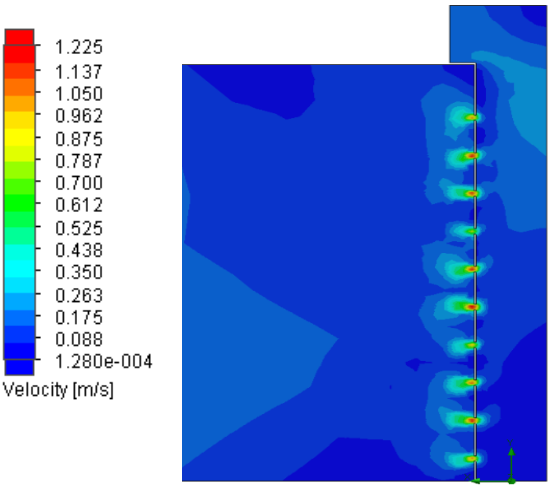

Figure 9. Average velocity gradient to Mesh 01

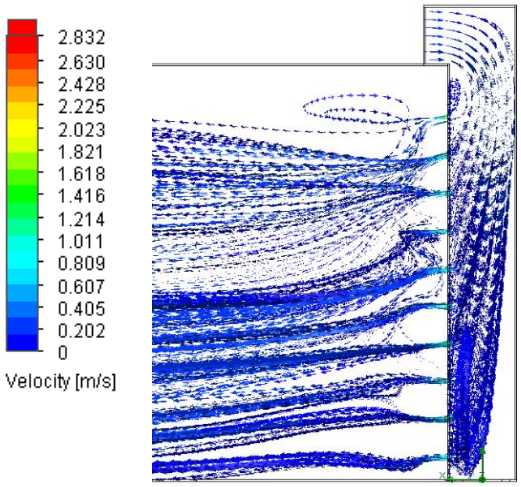

Figure 10. Air trajectory in the lateral duct to Mesh 01

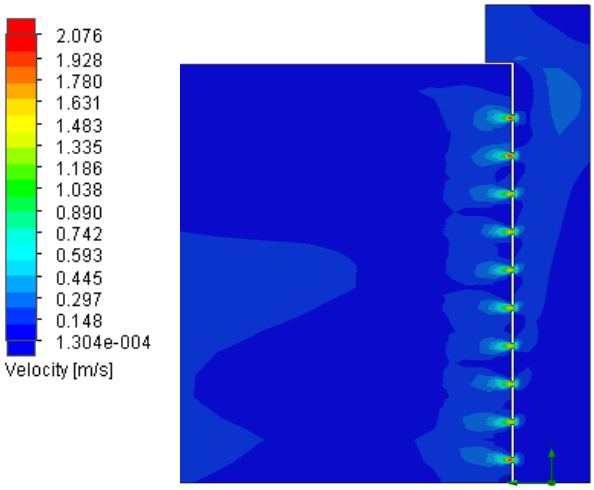

Figure 11. Average velocity gradient to Mesh 02

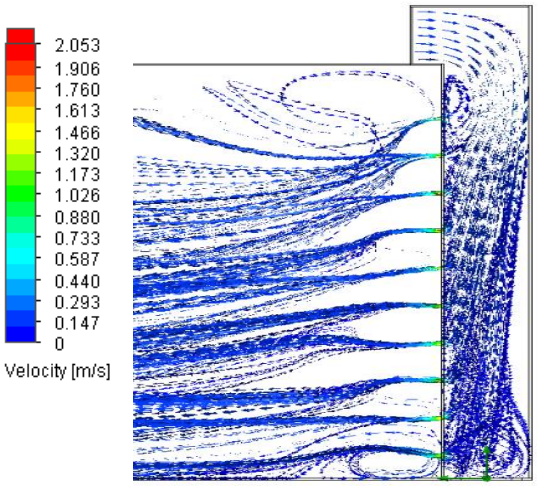

Figure 12. Air trajectory in the lateral duct to Mesh 02

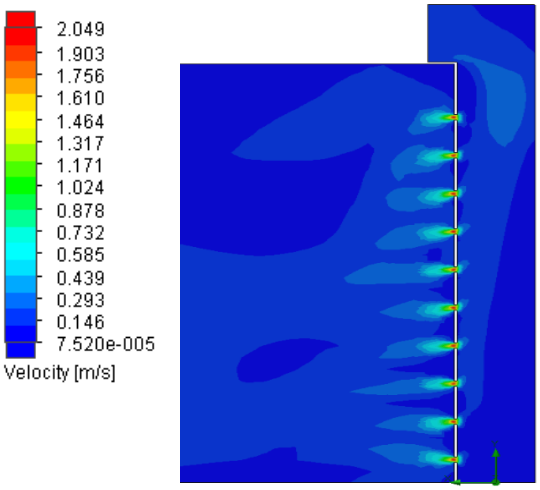

Figure 13. Average velocity gradient to Mesh 03

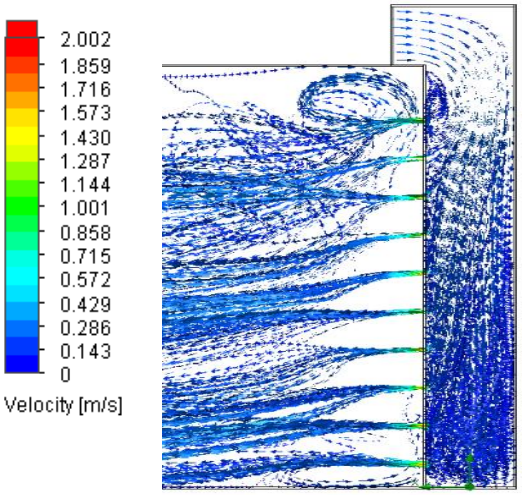

Figure 14. Air trajectory in the lateral duct to Mesh 03

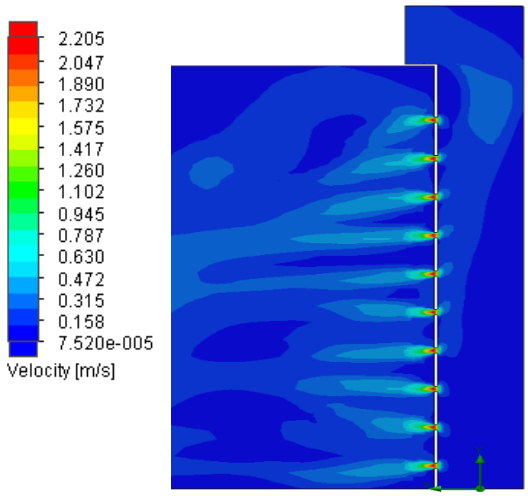

Figure 15. Average velocity gradient to Mesh 04

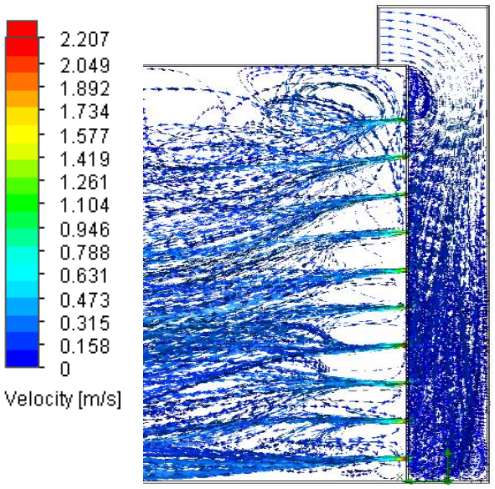

Figure 16. Air trajectory in the lateral duct to Mesh 04

It is observed in Fig. 9, 11, 13 and 15 that the refinement level of the adjustment gradient meshes for the exit of the duct openings to the environment. In mesh 03 and 04 the air jet has a higher definition favoring a possible incidence in the object located inside the chamber. In addition, in mesh 03 and 04 the velocity gradients have no homogeneity, which allows to visualize a mixture of flows caused by different directions of the vectors at the openings exit.

The Fig. 10, 12, 14 and 16 show the evolution of air trajectories, as a function of the meshes refinement. In the meshes 03 and 04 there is a formation of vortices at the input of air in the duct. In the lower part of the duct, because it is closed, the air current flows in and returns, interfering in the air jet direction.

3.2 Comparison of results through a single average path and across multiple paths

As a first comparative, a single average air path was developed, from the side duct input to the output openings, as shown in Fig. 17.

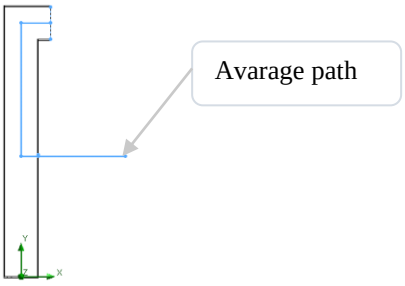

Figure 17. Middle path model single in the lateral duct

The data obtained by the simulation were compared with the experimental data collected in the industrial tunnel and presented in Fig. 18.

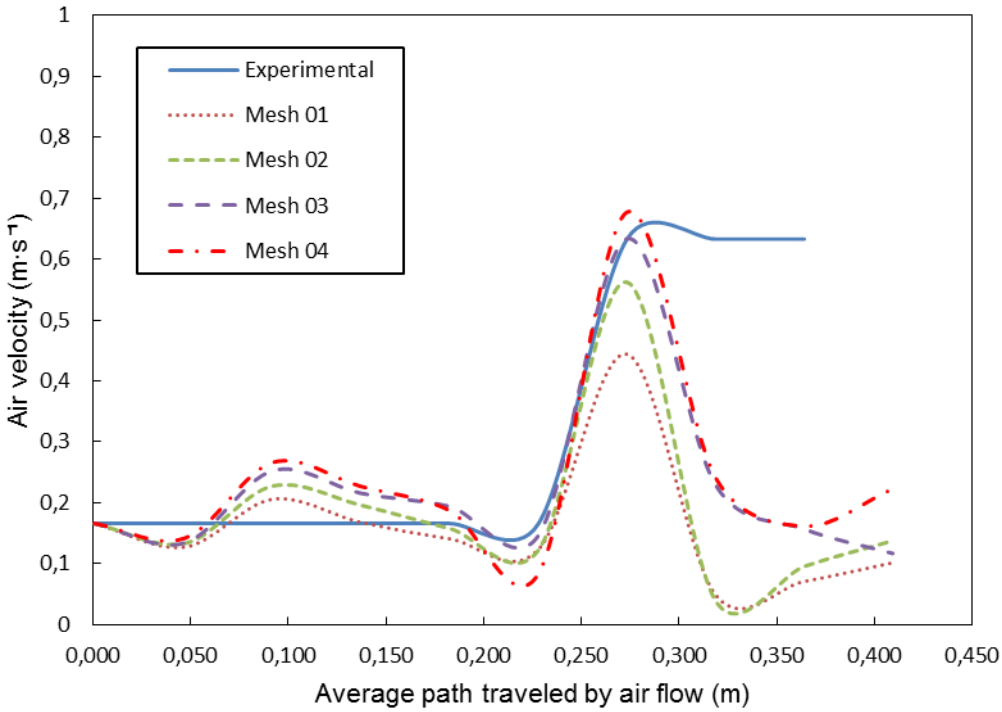

Figure 18. Comparison between experimental data and mesh to single average path

The meshes behavior compared with the experimental data presented oscillation in some points. The behavior closer to the experimental data in the openings exits was the mesh 03. At this point, there is the air flow to environment and all the meshes presented a different behavior from experimental data, since they were obtained in a closed chamber where there was recirculation, such behavior was expected.

The second comparison was made from thirteen paths distributed throughout the geometry as shown in Fig. 19. For each analyzed path, ten points were generated and each point provided an average velocity.

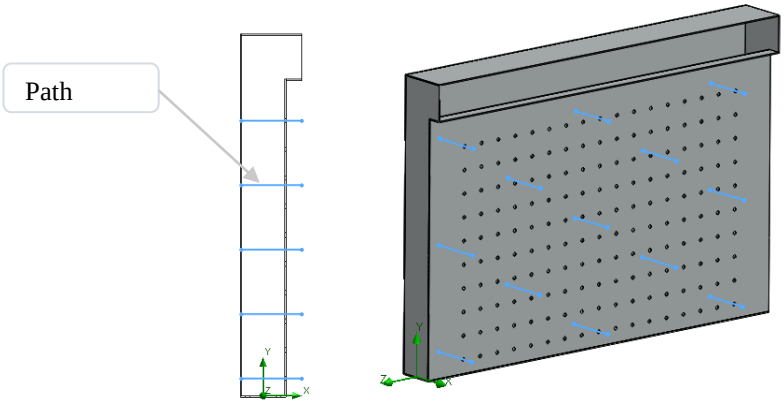

Figure 19. Multiple paths model in the lateral duct

The data obtained with the various mean paths for each mesh were compared to experimental data and presented in Fig. 20.

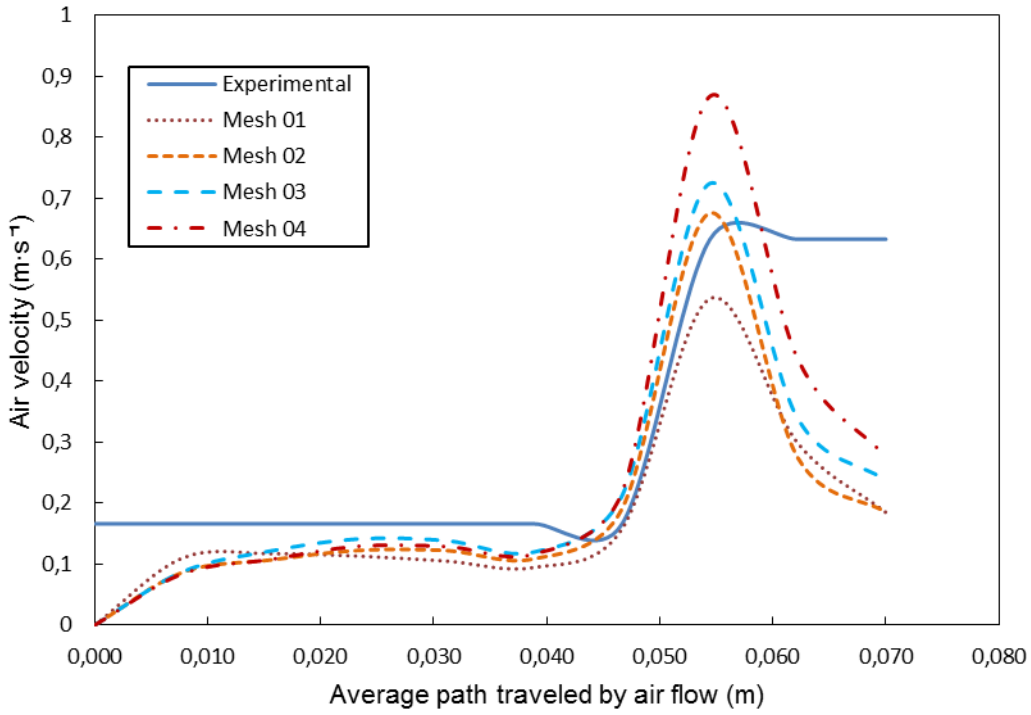

Figure 20. Comparison between experimental data and mesh to multiple paths

In Fig. 20 the meshes started with zero velocity because the paths started from the rear wall of the duct as shown in Fig. 19. When comparing the results generated by the thirteen paths with the experimental data it is observed that, at lower velocity, the meshes had similar behavior, while at higher velocity the mesh 2 presented better results. These results may have occurred due to the size and type of path analyzed that were different from the results of the analysis obtained considering only an average path.

3.3 Internal flow analysis

The Fig. 21 shows the result to air streamline inside the lateral duct and at chamber to mesh 3.

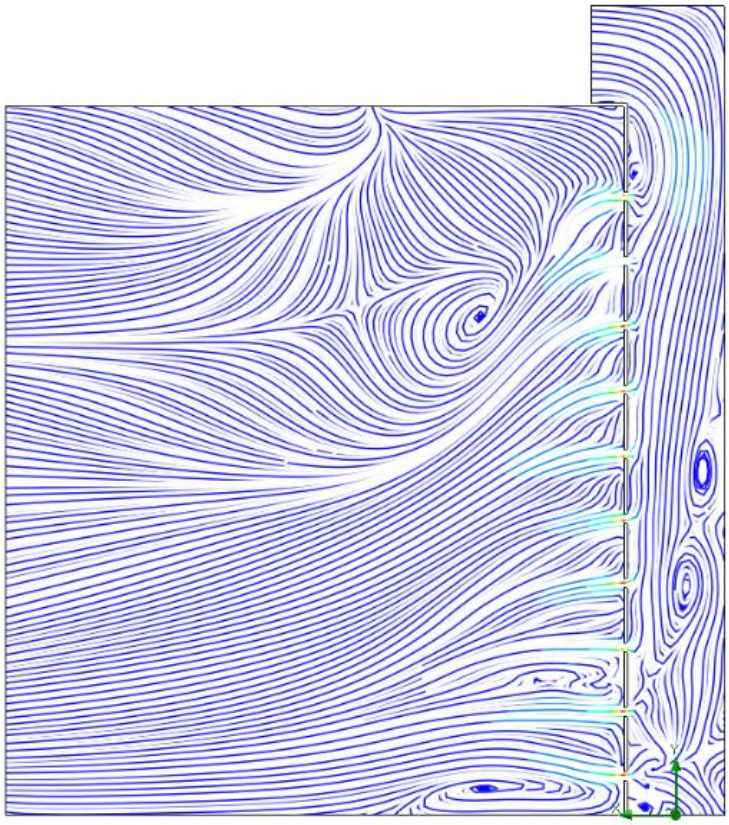

Figure 21. Air streamline to mesh 03.

Fig. 21 shows the formation of recirculation zones at various points in the duct, contraction at the input and expansion at the output S4. Systems with these behaviors were also found by Abd Rabbo *et al*. (2016), Majumdar (2011) and Innocenti *et al*. (2018) in their research about fluids internal flow, and Choudhry *et al*. (2015) that analyzed external flow. In his work, Duarte (2016) using Flow Simulation - version 2015, also found zones of contraction, recirculation and expansion of air internal flow.

4. CONCLUSIONS

Flow Simulation features an easy-to-understand computation implementation script optimizing use across diverse geometries. This system was fundamental to analysis to be performed quickly and without the need for a specific algorithm, using only the available platform.

When evaluating the simulation of air flow inside the lateral duct of term-shrinking tunnel, the results obtained through an individual path were different from results obtained with multiple paths. This is a consequence of the way paths are distributed, their sizes and number of analyzed points.

Through the single average path in the first mesh comparison at the exit of opening S4, mesh 03 was the one that most approached the experimental data, showing that it can be used to study this type of flow.

From the average input velocity, the flow inside the duct presents a recirculation, disfavoring the flow with greater homogeneity in the exit of openings due to variations in the air laminar trajectories.

As a suggestion for future works, simulation of flow and heat transfer in the chamber can be evaluated, as well as obtaining the experimental data for temperature gradient in order to optimize the equipment operation.

5. ACKNOWLEDGEMENTS

Thanks to Governo do Estado de Santa Catarina for support through the Programa de Bolsas Universitárias de Santa Catarina (UNIEDU) and Universidade Comunitária da Região de Chapecó – UNOCHAPECÓ.

6. REFERENCES

Abd Rabbo, M. F., Badawy, M. T. S., Sakr, R. Y., et al., 2016. *Numerical investigation of cutting edge effect on fluid*

flow and heat transfer for in-phase trapezoidal air channels. Alexandria Engineering Journal.

Bianchi, G., Rane, S., Kovacevic, A., Cipollone, R., 2017. *Deforming grid generation for numerical simulations of fluid dynamics in sliding vane rotary machines.* Advances in Engineering Software, vol. 112, p. 180–191.

Busto, S., Ferrín, J. L., Toro, E. F., Vázquez-Cendón, M. E., 2018. *A projection hybrid high order finite volume/finite element method for incompressible turbulent flows.* Journal of Computational Physics, vol. 353, n. October, p. 169–192.

Castorani, V., Landi, D., Germani, M., 2016. *Determination of the Optimal Configuration of Energy Recovery Ventilator through Virtual Prototyping and DoE Techniques*. Procedia CIRP, vol. 50, p. 52–57.

Choudhry, A., Arjomandi, M., Kelso, R., 2015. *A study of long separation bubble on thick airfoils and its consequent effects*. International Journal of Heat and Fluid Flow, vol. 52, p. 84–96.

Delgado, C. B., Silva, P. D., Pires, L. C., Gaspar, P. D., 2017. *Experimental study and numerical simulation of the interior flow in a telecommunications cabinet.* Energy Procedia. Anais... . vol. 142, p.3096–3101.

Driss, Z., Mlayeh, O., Driss, D., Maaloul, M., Abid, M. S., 2014. *Numerical simulation and experimental validation of the turbulent flow around a small incurved Savonius wind rotor*. Energy, vol. 74, n. C, p. 506–517.

Duarte, G. P. De P., 2016. *Estudo numérico e experimental do desempenho de atenuadores acústicos dissipativos de unidades de tratamento de ar*. Universidade Nova de Lisboa.

Fox, R. W., Mcdonald, A. T., 2014. *Introdução à mecânica dos fluídos*. LTC, Rio de Janeiro, 8 edition.

Frikha, S., Driss, Z., Hagui, M. A., 2015. *Computational study of the diffuser angle effect in the design of a waste heat recovery system for oil field cabins*. Energy, vol. 84, p. 219–238.

Jeong, W., Seong, J., 2014. *Comparison of effects on technical variances of computational fluid dynamics (CFD) software based on finite element and finite volume methods*. International Journal of Mechanical Sciences, vol. 78, p. 19–26.

Innocenti, A., Andreini, A., Bertini, D., Facchini, B., Motta, M., 2018. *Turbulent flow- field e ffects in a hybrid CFD-CRN model for the prediction of NO x and CO emissions in aero-engine combustors*. Fuel, vol. 215, n. December 2016, p. 853–864.

Kempe, T., Hantsch, A., 2017. *Large-eddy simulation of indoor air flow using an efficient finite-volume method*. Building and Environment, vol. 115, p. 291–305.

Lorusso, M., Capurso, T., Torresi, M., et al., 2017. *Efficient CFD evaluation of the NPSH for centrifugal pumps.* Energy Procedia, vol. 126, p. 778–785.

Majumdar, P., 2011. *Computational Fluid Dynamics Analysis of Turbulent Flow*. Computational Fluid Dynamics Technologies and Applications, Igor V. Minin and Oleg V. Minin, p. 255–292.

Mei, Y., Gong, S., Wang, C., et al., 2018. *Numerical simulation of drainage performance in a drain device of steam generator*. Annals of Nuclear Energy, vol. 114, p. 311–317.

Prah, B., Yun, R., 2017. *Heat Transfer and Flow Characteristics of CO2-Hydrate Mixture in Pipeline*. Energy Procedia, vol. 114, n. November 2016, p. 6813–6823.

Ragoth Singh, R., Nataraj, M., 2014. *Design and analysis of pump impeller using SWFS*. World Journal of Modelling and Simulation, vol. 10, n. 2, p. 152–160.

Ragoth Singh, R., Nataraj, M., Surendar, S., Siva, M., 2013 *Investigation of a centrifugal pump impeller vane profile using CFD*. International Review on Modelling and Simulations, vol. 6, n. 4.

Shrikant, A. A., Sivakumar, R., Vivekanandan, M., 2016. *Comparison of Shell and Tube Heat Exchanger using Theoretical Methods , HTRI , ASPEN and SOLIDWORKS simulation softwares*. Int. Journal of Engineering Research and Application, vol. 6, n. 3, p. 99–107.

Sobachkin, A., Dumnov, G., 2013. *Numerical Basis of CAD-Embedded CFD.* NAFEMS World Congress 2013, n. February, p. 1–20.

Stefan, K., Gunther, R., 2016. *CFD-Simulations in the Early Product Development. Procedia CIRP*, vol. 40, p. 443–448.

Turner, M.; Moxey, D.; Peiró, J.; et al., 2017. *A framework for the generation of high-order curvilinear hybrid meshes for CFD simulations.* Procedia Engineering, vol. 203, p. 206–218.

Wang, L., Fan, J., Zhao, W., 2017. *Flow Simulation and Strain Analysis of Active Guide Vane of Turbine based on Solidworks and CFD.* , vol. 32, p. 117–125.

7. RESPONSIBILITY NOTICE

The author(s) is (are) the only responsible for the printed material included in this paper.